Efficient IRS Deployment in IRS-Assisted OWC Networks Using a Circle Packing Algorithm

Juncheng Li*, Shenjie Huang§, Iman Tavakkolnia†, Harald Haas†, and Majid Safari*
*Institute for Imaging, Data and Communications, School of Engineering, The University of Edinburgh, Edinburgh, UK
§pureLiFi Ltd, Edinburgh, UK
†LiFi R&D Centre, Electrical Engineering Division, University of Cambridge, Cambridge, UK

***Abstract*—Laser-based optical wireless communication (OWC) can provide ultra-high-speed mobile connectivity for future networks. To address the misalignment challenges inherent in laser-based OWC systems, this paper introduces a novel intelligent reflecting surface (IRS)-assisted indoor OWC system. This system employs a multi-cell architecture and leverages passive IRS elements to enhance user coverage. The concept of angular coverage in indoor laser-based communication is introduced, and an analytical framework is proposed to calculate the angular coverage probability of users. Additionally, an innovative IRS deployment strategy, inspired by circle-packing principles, is proposed to enhance the angular coverage of users with varying locations and orientations. Numerical results validate the proposed IRS deployment strategy, demonstrating its superior performance compared to a conventional laser-based OWC architecture, achieving at least a threefold improvement in angular coverage probability.**

I. Introduction

Due to the increasing reliance on wireless communications, a range of critical challenges have emerged, including insufficient available radio spectrum, significant energy consumption, limited data rates, and security concerns. Indoor optical wireless communication (OWC), also known as light-fidelity (LiFi), is seen as a promising technology capable of effectively addressing these challenges and enabling high-speed transmission for future indoor mobile networks. Traditional implementations of LiFi rely on connections established through light-emitting diode (LED) transmitters, which have limited bandwidth and result in constrained data rates. To overcome this limitation and unlock the full potential of LiFi, LiFi 2.0 has been proposed, demonstrating the potential to support terabit-per-second (Tb/s) aggregate data transmission [1]. In particular, it has been shown that vertical cavity surface emitting lasers (VCSELs), which offer several advantages—such as high-speed direct modulation, high power conversion efficiency, and cost-effectiveness-can be employed to achieve high-speed indoor wireless transmission while adhering to safety limits for human eyes. In recent studies on laser-based indoor communication, researchers have primarily focused on ensuring positional coverage for users [2]–[4]. However, in practical scenarios, laser-based LiFi systems are particularly susceptible to misalignment losses caused by random receiver orientations and user mobility [5].

Motivated by the recent advances in intelligent reflective surfaces (IRS)-aided RF wireless communication, optical IRSs and smart optics have been proposed to enhance the stability of various OWC systems [6]. For instance, [7] investigates the potential of IRS technology to relax the line-of-sight (LoS) requirement in free-space optical communication (FSO) systems. In addition, [8] quantifies the performance improvements achieved through IRS integration in underwater OWC. Furthermore, the authors of [9] explore how the synergy between IRSs and LiFi can enable innovative applications by introducing intelligence into both transceiver operations and the surrounding environment.

While various studies have demonstrated the effectiveness of utilizing IRS to mitigate misalignment issues, notable research gaps still exist in the field of IRS-assisted indoor OWC. For example, the optimal deployment strategy for IRSs in laser-based OWC, supporting users with random locations and orientations, remains unexplored. Moreover, recent studies often rely on active IRSs, increasing system complexity and latency. In [10], IRS elements centralized on the wall can automatically adjust their orientation. However, given the limited beam size and high directivity of lasers, this architecture is ineffective in enhancing the outage performance of laser-based OWC systems. Moreover, accurate user location information is required to configure IRS orientation, making the system vulnerable to performance degradation due to positioning errors and latency introduced by IRS resource allocation and deployment. In [11], the authors propose a novel IRS-assisted LiFi system where the user can receive signals at any location and orientation. However, this system is developed for a single-user scenario, and the orientation of all IRS elements is adjustable to reflect the beam to any position in the room, resulting in high system complexity.

To address the aforementioned research gaps in indoor laser-based LiFi systems and promote its adoption in future sixth-generation (6G) technology, this study proposes a novel IRS-assisted LiFi system with a multi-cell architecture and passive IRS elements to mitigate misalignment issues. Specifically, we introduce a downlink laser-based LiFi system that delivers high-speed wireless connectivity with low outage probability, regardless of the random location or orientation of user equip-

This work was supported by the Engineering and Physical Sciences Research Council (EPSRC) through the TOWS under Grant EP/S016570/1 and through the TITAN under Grant EP/X04047X/1 and Grant EP/Y037243/1.

ments (UEs). Additionally, we propose an innovative algorithm for the optimal deployment of IRS elements to enhance angular coverage. To the best of our knowledge, this study is the first to introduce the concept of angular coverage in indoor laser-based OWC systems.

II. System Model

In a recent study [3] on indoor laser-based communication, a centralized access point (AP) architecture using arrays of VCSELs is considered to support communication channels across the entire room. Successful data transmission requires the UE with a limited field-of-view (FoV) to be oriented towards the optical AP. However, meeting this requirement is challenging in practical mobile wireless communication scenarios, as UEs often move unpredictably with varying orientations. Therefore, to maintain connectivity regardless of user behavior, it is essential to provide optical signals from multiple directions. In our proposed indoor IRS-assisted LiFi system, the room is divided into $N_{\mathrm{c}} \times N_{\mathrm{c}}$ square cells. A total of $N_{\mathrm{I}} \times N_{\mathrm{c}}^2$ fully-passive IRS elements are deployed on the walls, organized into N_{c}^2 groups. Each group consists of N_{I} IRS elements, serving a single cell. Furthermore, each IRS element is illuminated by a dedicated laser mounted on the ceiling. Consequently, the system provides, for each cell, N_{I} IRS-enabled non-line-of-sight (NLoS) links along with one line-of-sight (LoS) link via the AP. Note that the fully passive IRSs used in this paper consist of optical mirrors mounted on walls with fixed orientations, resulting in a constant direction for the reflected beam.

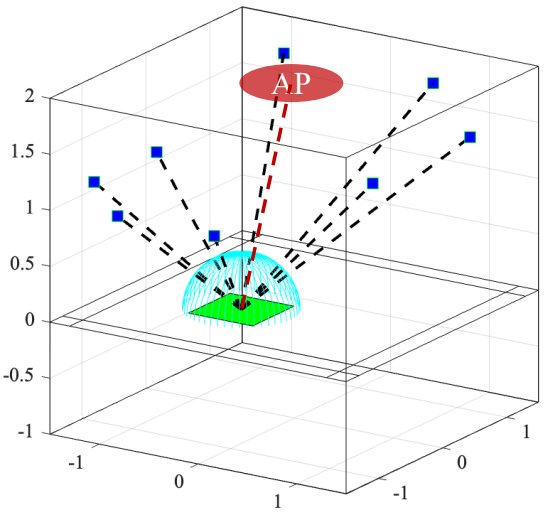


Fig. 1. The proposed IRS-assisted LiFi system. The blue squares represent the IRS elements.

A. IRS-Assisted System Architecture

To control the complexity of the designs and evaluate the impact of deploying IRS elements fairly with respect to a conventional design, we set the total number of lasers (used for LoS and NLoS links) not exceeding a fixed constant denoted by N_{L}. Thus, as the number of sources (AP and IRS) serving each cell changes, the number of cells must be adjusted accordingly, which also results in changes to the cell size. This constraint is mathematically expressed as

$$N_{\mathrm{s}} N_{\mathrm{c}}^2 \leq N_{\mathrm{L}}, \tag{1}$$

where $N_{\mathrm{s}} = N_{\mathrm{I}} + 1$ is the number of sources serving each cell (including N_{I} lasers for IRS-assisted NLoS links and one laser for LoS link), N_{c}^2 is the total number of cells. Note that in the case without IRS, $N_{\mathrm{s}} = 1$, and the number of cells equals the number of available lasers, i.e., $N_{\mathrm{c}}^2 = N_{\mathrm{L}}$.

Fig. 1 shows the proposed IRS-assisted design, where the locations of the AP and 8 passive IRSs allocated for a specific (green) cell are illustrated. In this work, the spherical coordinate system is used to analyze device orientation, where the polar angle $\theta \in [0, \pi]$ is defined as the angle between the normal vector of the user equipment (UE) and the positive z-axis, and the azimuth angle $\phi \in [0, 2\pi)$ represents the angle between the projection of the normal vector on the xy-plane and the positive x-axis. Note that the blue hemisphere in Fig. 1 shows the spherical coordinate centered at the cell's center.

B. Coverage Solid Angle and Angular Coverage Probability

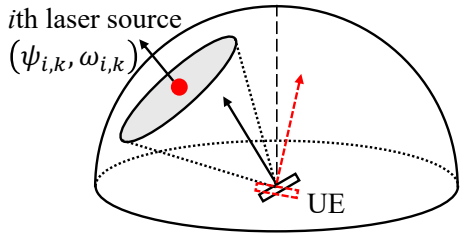


Fig. 2. The angular coverage solid angle is indicated by the shaded cone with apex angle of FoV. The black and the red dashed arrows illustrate examples of the UE's orientation where the signal can and cannot be received, respectively.

In this paper, the UE is assumed to be covered by a source, whether it is the AP or the IRS, if the UE is located within the laser beam spot and the laser source is within the receiver FoV. If we define a spherical coordinate system for the kth cell ($1 \leq k \leq N_{\mathrm{c}}^2$) with the cell center as the origin, and place the ith laser source (AP or IRS) at $(\psi_{i,k}, \omega_{i,k})$, the coverage angle is represented by a solid angle centered at $(\psi_{i,k}, \omega_{i,k})$ with a size equal to half of the FoV, as shown in Fig. 2. It is important to note that distance is not a factor in this study since the received SNR is not considered. The location of the laser, as discussed here, refers specifically to its direction relative to the center of the cell. Therefore, a UE is considered covered by the source as long as the angle between the device's orientation and the direction $(\psi_{i,k}, \omega_{i,k})$ is smaller than FoV/2. For instance, assuming the device orientation is uniformly distributed across the hemispherical coordinate system, the coverage probability provided by a single source is given by $P_{\mathrm{c}} = \frac{\Omega(\mathrm{FoV})}{2\pi}$, where $\Omega(\mathrm{FoV}) = 2\pi(1 - \cos(\mathrm{FoV}/2))$ is the solid angle defined by the FoV of the UE. It is important to note that the distance between the UE and the source does

not impact our coverage analysis, as we do not consider the received signal-to-noise ratio (SNR) in defining the angular coverage.

Assuming there are N_{s} sources serving a cell and the polar angle θ and the azimuth angle ϕ of the UE follow a joint probability density function (PDF) $f_{\Theta,\Phi}(\theta,\phi)$, the angular coverage probability can be expressed as:

$$P_{\mathrm{c},k} = \iint_{\mathbf{R}(\Omega_{1,k}\cup\ldots\cup\Omega_{N_{\mathrm{s}},k})} f_{\Theta,\Phi}(\theta,\phi)\,\mathrm{d}\theta\mathrm{d}\phi, \tag{2}$$

where $\Omega_{i,k}$ represents the coverage solid angle of the ith source in the kth cell, defined as:

$$\Omega_{i,k} = \left\{ (\theta,\phi) \,\middle|\, \arccos\left(\mathbf{u}^{\mathrm{T}}\mathbf{w}_{i,k}\right) \le \frac{\mathrm{FoV}}{2} \right\}, \tag{3}$$

where

$$\mathbf{w}_{i,k} = \begin{bmatrix} \sin(\psi_{i,k})\cos(\omega_{i,k}) \\ \sin(\psi_{i,k})\sin(\omega_{i,k}) \\ \cos(\psi_{i,k}) \end{bmatrix}, \quad \mathbf{u} = \begin{bmatrix} \sin(\theta)\cos(\phi) \\ \sin(\theta)\sin(\phi) \\ \cos(\theta) \end{bmatrix}.$$

The $\mathbf{w}_{i,k}$ and $\mathbf{u}$ are the direction vector of the laser source and the user orientation. Also in (2), $\mathbf{R}(\Omega_{1,k}\cup\ldots\cup\Omega_{N_{\mathrm{s}},k})$ denotes the total coverage solid angle created by N_{s} sources.

Since finding an analytical expression for the coverage probability with multiple sources is complex, here we only derive the mathematical expression for the coverage probability of a single source and simulate multiple-source scenarios. Considering that the ith source is located at $\left(x_{\mathrm{s},i}^{(k)}, 0, z_{\mathrm{s},i}^{(k)}\right)$, where $x_{\mathrm{s},i}^{(k)} \ge 0$ and $z_{\mathrm{s},i}^{(k)} \ge 0$, in a Cartesian coordinate system, we first rotate the spherical system so that the source is located at $\left(0, 0, z_{\mathrm{s},i}^{(k)}\right)$ to facilitate calculations. In the rotated system corresponding to the ith source:

$$\begin{aligned} x_i^{(k)} &= x\cos(\psi_{i,k}) - z\sin(\psi_{i,k}), \\ y_i^{(k)} &= y, \\ z_i^{(k)} &= x\sin(\psi_{i,k}) + z\cos(\psi_{i,k}), \end{aligned}$$

where $\psi_{i,k} = \arctan\left(\frac{x_{\mathrm{s},i}^{(k)}}{z_{\mathrm{s},i}^{(k)}}\right)$. Converting the transformed Cartesian coordinates back to the original spherical coordinates, we get the following equations:

$$\begin{aligned} \theta = g(\theta_{i,k},\phi_{i,k}) = \arccos\big[&\cos(\theta_{i,k})\cos(\psi_{i,k}) \\ &- \sin(\theta_{i,k})\cos(\phi_{i,k})\sin(\psi_{i,k})\big], \end{aligned} \tag{4}$$

$$\begin{aligned} \phi = h(\theta_{i,k},\phi_{i,k}) = \mathrm{atan2}\big[&\sin(\theta_{i,k})\sin(\phi_{i,k}), \\ &\sin(\theta_{i,k})\cos(\phi_{i,k})\cos(\psi_{i,k}) + \cos(\theta_{i,k})\sin(\psi_{i,k})\big]. \end{aligned} \tag{5}$$

The joint PDF of the new variables $(\theta_{i,k},\phi_{i,k})$ after coordinate rotation can be found using the following formula based on the Jacobian determinant:

$$\begin{aligned} &f_{\Theta_{i,k},\Phi_{i,k}}(\theta_{i,k},\phi_{i,k}) \\ &\quad = f_{\Theta,\Phi}\left(g(\theta_{i,k},\phi_{i,k}), h(\theta_{i,k},\phi_{i,k})\right)\cdot|\mathbf{J}_{i,k}|, \end{aligned} \tag{6}$$

where

$$|\mathbf{J}_{i,k}| = \begin{vmatrix} \frac{\partial g(\theta_{i,k},\phi_{i,k})}{\partial\theta_{i,k}} & \frac{\partial g(\theta_{i,k},\phi_{i,k})}{\partial\phi_{i,k}} \\ \frac{\partial h(\theta_{i,k},\phi_{i,k})}{\partial\theta_{i,k}} & \frac{\partial h(\theta_{i,k},\phi_{i,k})}{\partial\phi_{i,k}} \end{vmatrix} \tag{7}$$

is the Jacobian determinant representing the area scaling factor resulting from the transformation of variables from (θ,ϕ) to $(\theta_{i,k},\phi_{i,k})$. After obtaining the transformed PDF, we can directly calculate the coverage probability for a single source by integrating $\theta_{i,k}$ from 0 to $\frac{\mathrm{FoV}}{2}$ and $\phi_{i,k}$ from 0 to 2π:

$$P_{\mathrm{c},i}^{(k)} = \int_0^{2\pi}\int_0^{\frac{\mathrm{FoV}}{2}} f_{\Theta_{i,k},\Phi_{i,k}}(\theta_{i,k},\phi_{i,k})\mathrm{d}\theta_{i,k}\mathrm{d}\phi_{i,k}. \tag{8}$$

C. Circle Packing on a Spherical Cap

Note that the intersection of the coverage solid angles of each source forms a circle on the surface of the spherical cap, defining the angular region of interest. The angular coverage is maximized when the circles created by all sources serving each cell cover the maximum possible area on this spherical cap [12]. Therefore, our proposed algorithm draws inspiration from the circle packing problem, which aims to find the maximum circle radius for a given number of non-overlapping circles packed on a unit sphere. In the following sections, the distributed AP configuration is assumed, i.e., the AP is positioned directly above each cell. Thus, due to symmetry, the IRS deployment (described by the polar coordinates at the center of each cell) is identical for all cells, allowing the parameter k to be removed from our notation in the following derivations.

Assuming α_{ij} is the angular distance between the centers of ith and the jth circles, it can be expressed as:

$$\alpha_{ij} = \arccos\left(\mathbf{w}_i^{\mathrm{T}}\mathbf{w}_j\right), \tag{9}$$

Therefore the circle packing optimization in our scenario can be expressed as follows:

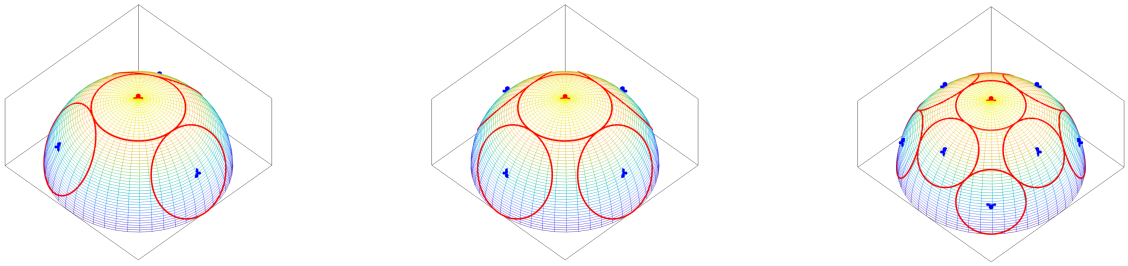
$$\begin{aligned} \text{Maximize} \quad & D \\ \text{subject to} \quad & \forall i,j\in\mathbb{Z}, 1\le i,j\le N_{\mathrm{I}}, \quad 0\le\psi_i,\psi_j\le\theta_{\mathrm{b}}, \\ & \forall i,j\in\mathbb{Z}, 1\le i,j\le N_{\mathrm{I}}, \quad 0\le\omega_i,\omega_j<2\pi, \end{aligned} \tag{10}$$

where $D = \min\{\alpha_{ij} \mid 1\le i<j\le N_{\mathrm{s}}\}$ is the minimum angular distance between all the circles, which also corresponds to the diameter of the circles. Assuming that the polar angles associated with the edges of the circles do not exceed $\frac{\pi}{2}$, we can express $\theta_{\mathrm{b}} = \frac{\pi-D}{2}$, which represents the boundary of the polar angles in this case.

The optimization problem in (10) can be solved numerically, demonstrating that for $N_{\mathrm{s}} = 4, 5$, and 9, the optimal azimuth angles are such that the circles are uniformly distributed across the azimuth angle range of $[0, 2\pi)$, i.e.,

$$\omega_i^{\dagger} = \frac{\pi}{N_{\mathrm{I}}}(i-1), \quad i\in\mathbb{Z}, 1\le i\le N_{\mathrm{I}}. \tag{11}$$

The optimal value of ψ_i varies depending on the value of N_{s}. In this paper, we focus on $N_{\mathrm{s}} = 4, 5$ and 9, which fit well with the total number of sources per cell considered for the



(a) 4 circles, $D^\dagger = \frac{\pi}{3}$ (b) 5 circles, $D^\dagger = \frac{\pi}{3}$ (c) 9 circles, $D^\dagger = 0.2428\pi$

Fig. 3. Circle packing on semi-sphere with different number of circles.

underlying scenario. For $N_\mathrm{s} = 4$ and 5, the circle packing solution indicates that the circles are positioned in a single layer along the same polar angle. Therefore, as observed in Fig. 3 (a) and (b), the polar angle $\psi_i^\dagger$ and the corresponding $D^\dagger$ are equal and satisfy

$$D^\dagger = \psi_i^\dagger = \theta_\mathrm{b}^\dagger, \quad i \in \mathbb{Z}, 1 \le i \le N_\mathrm{I}. \tag{12}$$

Noting the definition $\theta_\mathrm{b} = \frac{\pi - D}{2}$, (12) leads to $\theta_\mathrm{b}^\dagger = \theta_{\mathrm{b}0} = \frac{\pi}{3}$, $D^\dagger = D_0^\dagger = \frac{\pi}{3}$, and $\psi_{i0}^\dagger = \frac{\pi}{3}$ for $N_\mathrm{s} = 4$ and 5. Similarly, for $N_\mathrm{s} = 9$, the circle-packing results indicate that the circles are positioned at two layers, defined by two different polar angles as observed in Fig. 3 (c). Therefore, the optimal solution to (10) can be determined geometrically for the two layers (represented by odd and even values of i) as

$$\psi_i^\dagger = \begin{cases} D^\dagger, & i \text{ is odd and } 1 \le i \le N_\mathrm{I}, \\ \theta_\mathrm{b}^\dagger, & i \text{ is even and } 1 \le i \le N_\mathrm{I}, \end{cases} \tag{13}$$

with

$$D^\dagger = \arctan\left[\frac{1 - \cos\left(\theta_\mathrm{b}^\dagger\right)}{\frac{\sqrt{2}}{2}\sin\left(\theta_\mathrm{b}^\dagger\right)}\right]. \tag{14}$$

Hence, using the definition of $\theta_\mathrm{b} = \frac{\pi - D}{2}$, for $N_\mathrm{s} = 9$, we can calculate $\theta_\mathrm{b}^\dagger = \theta_{\mathrm{b}0} = 0.3786\pi$, $D^\dagger = D_0^\dagger = 0.2428\pi$, and

$$\psi_{i0}^\dagger = \begin{cases} 0.2428\pi, & i \text{ is odd and } 1 \le i \le N_\mathrm{I}, \\ 0.3786\pi, & i \text{ is even and } 1 \le i \le N_\mathrm{I}. \end{cases} \tag{15}$$

These results are shown in Fig. 3 for $N_\mathrm{s} = 4$, 5, and 9, which will be used in our IRS deployment algorithm in section III.

III. IRS Deployment Design

This section presents the IRS deployment design, which aims to meet the high angular coverage requirements defined in the last section. Given constraints such as limited beam size, restricted FoV, and other practical limitations, achieving full coverage in the strictest sense might not be feasible. Therefore, this study adopts the following three pragmatic and justifiable assumptions: (a) the height of the device is set to $1\,\mathrm{m}$; (b) the distance between the UE and the walls is always at least d_UW; (c) the mobile device is never oriented downward, i.e., $\theta \in [0, \pi/2]$, since the AP is always installed higher than the user's active region.

The proposed design aims at maximizing angular coverage probability—that is, the total coverage solid angle of the AP and all IRS elements over the solid angle of the hemisphere 2π, as described by (2):

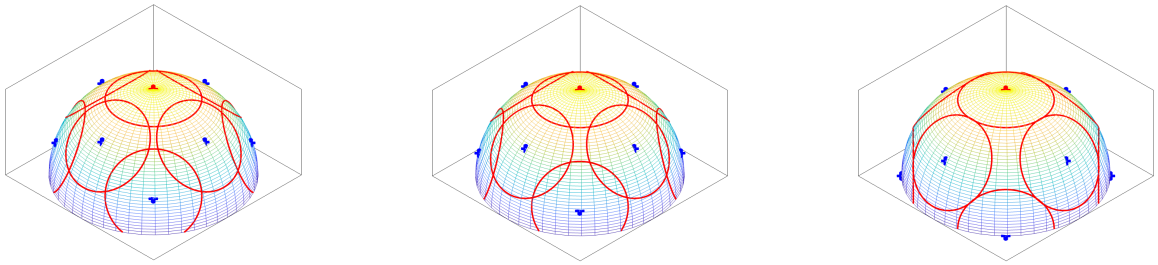
$$\begin{aligned} P_\mathrm{c} &= \iint_{\mathbf{R}(\Omega_1 \cup \ldots \cup \Omega_{N_\mathrm{s}})} \frac{\sin(\theta)}{2\pi} \mathrm{d}\theta \mathrm{d}\phi, && 0 \le \theta \le \frac{\pi}{2}, \\ &= \frac{\mathbf{R}\left(\Omega_1 \cup \ldots \cup \Omega_{N_\mathrm{s}}\right)}{2\pi}, && 0 \le \theta \le \frac{\pi}{2}. \end{aligned} \tag{16}$$

Note that the angular coverage probability is also the coverage probability of a UE with uniform orientation distribution based on (8).

The angular location of the ith circle, $(\psi_i^\dagger, \omega_i^\dagger)$ shown in Fig. 3 is calculated based on the circle packing optimization. These results correspond to optimal IRS deployment when receiver FOV equals the maximum diameter of non-overlapping circles packed in the spherical cap, i.e., $\mathrm{FoV} = D_0^\dagger$. More generally, when $\mathrm{FoV} \le D_0^\dagger$ the values $\psi_i = \psi_i^\dagger$ and $\omega_i = \omega_i^\dagger$ still yield an optimal solution, since there would be no overlap between the coverage circles with diameters smaller than the circle-packing solution, resulting in an overall angular coverage of $N_\mathrm{s}\Omega(\mathrm{FoV})$. However, circles with diameters equal to $\mathrm{FoV} > D_0^\dagger$ placed at the positions $(\psi_i^\dagger, \omega_i^\dagger)$ would overlap, resulting in coverage inefficiency. Therefore, the positions $(\psi_i^\dagger, \omega_i^\dagger)$ would no longer necessarily be optimal. Therefore, we propose a suboptimal circle-packing-based algorithm for the case of $\mathrm{FoV} > D_0^\dagger$, considering two possible modifications to the original circle-packing solution to improve the coverage probability:

Spherical Cap Expansion: This approach aims to avoid overlap among the coverage circles while increasing the FoV. Therefore, it requires expanding the circle packing space by increasing θ_b (e.g., see Fig. 4(c)). This maintains the efficiency of non-overlapping coverage circles while enhancing the coverage closer to the boundary of the spherical cap, i.e., $\theta = \frac{\pi}{2}$. However, the covered angles beyond $\theta = \frac{\pi}{2}$ would be outside the angular region of interest, leading to some coverage inefficiency.

Overlapping Circle Packing: This approach allows for some level of overlap among coverage circles by fixing the posi-



(a) $\beta = 0$ (keep at $\psi_{i0}^{\dagger}$). (b) $\beta = 0.3$. (c) $\beta = 1$ (no overlap).

Fig. 4. IRS locations for different β when $N_{\mathrm{I}} = 8$ and $\mathrm{FoV} = 55^{\circ}$ (red point: AP; blue points: IRS).

tion of the circles based on the circle packing solution, but expanding the size of the circles. This would lead to some coverage inefficiency in overlapping areas, but it can also improve the angular coverage by closing the uncovered gaps among coverage circles (e.g., see Fig. 4(a)).

There is an inherent trade-off between these two strategies and we propose a hybrid approach to effectively exploit this trade-off (e.g., see Fig. 4(b)). As indicated before, a circle-packing solution with coverage circles of diameter $\mathrm{FoV} > D_0^{\dagger}$ can only exist, if the boundary of polar angles in (10) expands beyond $\theta_{\mathrm{b}0}$ (i.e., first strategy). However, for a large FoV and larger number of IRS sources, the circle-packing solution with the expanded boundary would lead to excessive coverage inefficiency. We, therefore, define a scaling parameter $\beta \in [0, 1]$ and solve the circle-packing problem considering a smaller coverage circle with the scaled diameter

$$D_{\mathrm{S}} = \beta \left(\mathrm{FoV} - D_0^{\dagger} \right) + D_0^{\dagger}, \quad \mathrm{FoV} > D_0^{\dagger}, \tag{17}$$

which varies in the range $D_0^{\dagger} \leq D_{\mathrm{S}} \leq \mathrm{FoV}$ as β changes from 0 to 1. We then fix the angular position of the IRS sources based on the solution of this circle-packing problem (i.e., (ψ_i^*, ω_i^*)), and finally expand the diameter of the coverage circles centered at (ψ_i^*, ω_i^*)) from D_{S} to FoV. This final step would result in an overlapping circle-packing solution (i.e., second strategy).

Let us denote θ_{b}^* as the expanded boundary of polar angles required to achieve a solution with non-overlapping circles of diameter $D_{\mathrm{S}}(\mathrm{FoV})$ in problem (10). Then, considering (12), we can readily write the solution of the circle-packing problem for for $N_{\mathrm{s}} = 4$ and 5 as $\psi_i^* = \theta_{\mathrm{b}}^* = D_{\mathrm{S}}(\mathrm{FoV})$. Here, we also make a practical assumption that the IRS sources are not placed below the height of UE (i.e., $\psi_i^* \leq \frac{\pi}{2}$). Considering this assumption, the solution becomes

$$\psi_i^* = \theta_{\mathrm{b}}^* = \min \left\{ D_{\mathrm{S}}, \frac{\pi}{2} \right\}. \tag{18}$$

Similarly, for $N_{\mathrm{s}} = 9$, considering diameter of D_{S} for circle packing problem, the expanded boundary can be calculated by solving (14) as:

$$\theta_{\mathrm{b}}^* = \min \left\{ \arcsin \left(\frac{\sqrt{2} \tan\left(D_{\mathrm{S}}\right)}{\tan^2\left(D_{\mathrm{S}}\right)/2 + 1} \right), \frac{\pi}{2} \right\}, \tag{19}$$

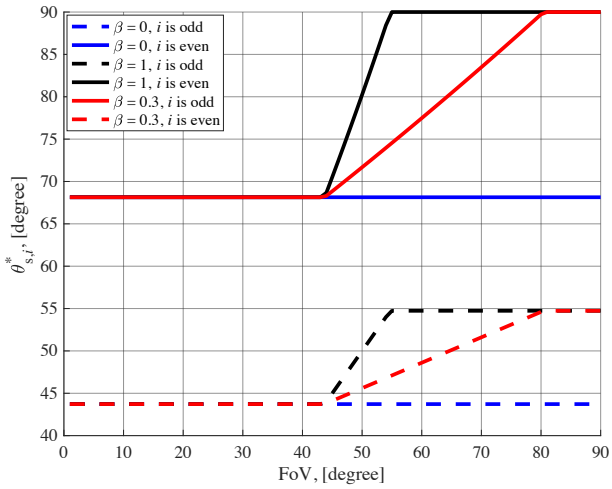


Fig. 5. IRS polar angle ψ_i^* versus FoV based on different β for $N_{\mathrm{I}} = 8$.

Algorithm 1 IRS configuration design

Input: FoV, N_{c}, β
Output: ψ_i^*, ω_i^*
1: **if** $\mathrm{FoV} \leq D^{\dagger}$ **then**
2: $\psi_i^* \leftarrow \psi_i^{\dagger}$ based on (12) or (13)
3: **else**
4: Calculate D_{S} based on (17)
5: Calculate ψ_i^* based on and (19) or (20)
6: **end if**
7: $\omega_i^* \leftarrow \omega_i^{\dagger}$ based on (11)
8: **return** ψ_i^*, ω_i^*

where the practical limit of $\psi_i^* \leq \frac{\pi}{2}$ is also incorporated. Then, based on (13), the optimal solutions can be expressed as

$$\psi_i^* = \begin{cases} \min\left\{ D_{\mathrm{S}}, \arctan\left(\sqrt{2}\right) \right\}, & i \text{ is odd}, \\ \theta_{\mathrm{b}}^*, & i \text{ is even}, \end{cases} \tag{20}$$

where the bound $\arctan\left(\sqrt{2}\right)$ is obtained by inserting $\theta_{\mathrm{b}}^* = \frac{\pi}{2}$ in (14). The designed algorithm is presented in Algorithm 1, which gives the optimal locations of IRS elements, ψ_i^* and ω_i^*. The output ψ_i^* of the algorithm for different FoV values based on $\beta = 0$, 0.3, and 1 for $N_{\mathrm{s}} = 9$ is shown in Fig. 5. Note that

there are two distinct ψ_i^* values due to the two-tier structure of the circle packing arrangement shown in Fig. 4.

IV. Numerical Results and Discussions

This section presents the simulation results for the angular coverage probability of the proposed design. In the simulations, we assume that the user is uniformly distributed within the effective range $x_{\rm u} \in [-\frac{a}{2}+d_{\rm UW}, \frac{a}{2}-d_{\rm UW}]$, $y_{\rm u} \in [-\frac{a}{2}+d_{\rm UW}, \frac{a}{2}-d_{\rm UW}]$, at a UE height of $z_{\rm u}$, where a is the room side length. Additionally, the distributed AP configuration is considered in the simulations. We calculate the average angular coverage probability at different locations in the room and plot the average results as shown in Fig. 6. The parameters used in the simulations are listed in Table I. Notice that the selected β is 0.3, 0.2, and 0.1, for $N_{\rm c}=4$, $N_{\rm c}=5$, and $N_{\rm c}=6$ with uniform user orientation distribution, respectively. In general, β can be optimized with respect to FoV, but based on our numerical analysis, these fixed values of β represent good overall designs for various scenarios with different number of IRS sources.

TABLE I
Simulation Parameters

Symbols	Values	Descriptions
a	3 m	Room side length
h	3 m	Room height
$z_{\rm u}$	1 m	UE height
$d_{\rm UW}$	0.2 m	Minimum distance from the UE to the wall
β	0.3	$N_{\rm c}=4$
	0.2	$N_{\rm c}=5$
	0.1	$N_{\rm c}=6$

It is evident that the angular coverage increases as the FoV increases, due to the larger coverage angle of each source. Similarly, as we increase the cell size, i.e., increase the number of IRS elements serving each cell, we can also achieve higher angular coverage. However, it is evident from Fig. 6 that when the FoV is larger than the diameter of the original circle packing results $D_0^\dagger$ ($\theta_{\rm b}=\theta_{\rm b0}$) shown in Fig. 3 (i.e., FoV $=43.7^\circ$ for $N_{\rm c}=4$ and FoV $=60^\circ$ for $N_{\rm c}=5$), the growth rate of angular coverage probability slows down, due to the gradual overlap among the coverage angles of different IRS sources. However, in practical scenarios, optical receivers with large FoVs are less common. Therefore, the proposed circle-packing-based design remains optimal for most practical cases.

V. Conclusions

This paper proposes a novel IRS-assisted OWC system designed to mitigate misalignment issues through a multi-cell architecture and the use of passive IRS elements. Specifically, it introduces the concept of angular coverage in indoor laser-based communication and proposes an innovative IRS deployment strategy, inspired by circle packing principles, to ensure efficient angular coverage for ultra-high-speed laser-based wireless connectivity, regardless of random user locations and orientations. Numerical results confirm the effectiveness of the proposed IRS deployment strategy, showcasing its significant advantage over conventional laser-based OWC architectures and demonstrating a minimum threefold enhancement in angular coverage probability.

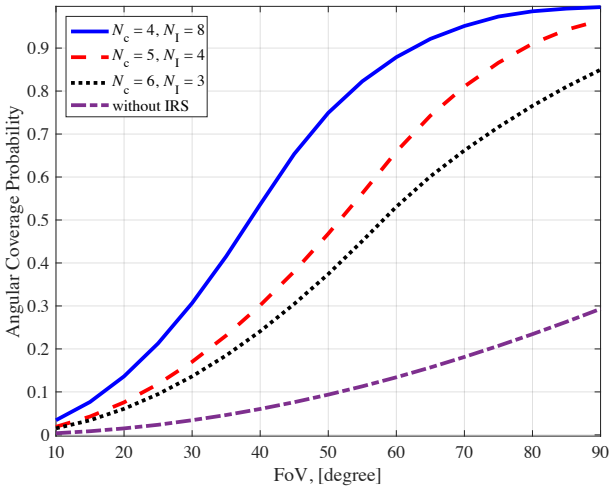


Fig. 6. Average angular coverage probability versus FoV.

References

[1] M. D. Soltani *et al.*, "Terabit indoor laser-based wireless communications: Lifi 2.0 for 6G," *IEEE Wireless Commun.*, vol. 30, no. 5, pp. 36–43, 2023.

[2] Y. Liu *et al.*, "High-capacity optical wireless VCSEL array transmitter with uniform coverage," in *Free-Space Laser Commun. XXXV*, vol. 12413. SPIE, 2023, pp. 144–150.

[3] H. Kazemi *et al.*, "A novel terabit grid-of-beam optical wireless multi-user access network with beam clustering," *arXiv preprint arXiv:2404.04443*, 2024.

[4] J. Li *et al.*, "Laser-based indoor mobile wireless communication aided by stabilizers," *IEEE Open J. Commun. Soc.*, vol. 5, pp. 7525–7541, 2024.

[5] M. D. Soltani *et al.*, "Modeling the random orientation of mobile devices: Measurement, analysis and LiFi use case," *IEEE Trans. Commun.*, vol. 67, no. 3, pp. 2157–2172, 2018.

[6] A. M. Abdelhady *et al.*, "Visible light communications via intelligent reflecting surfaces: Metasurfaces vs mirror arrays," *IEEE Open J. Commun. Soc.*, vol. 2, pp. 1–20, 2021.

[7] V. Jamali *et al.*, "Intelligent reflecting surface assisted free-space optical communications," *IEEE Commun. Mag.*, vol. 59, no. 10, pp. 57–63, 2021.

[8] Y. Ata *et al.*, "Intelligent reflecting surfaces for underwater visible light communications," *IEEE Photon. J.*, vol. 15, no. 1, pp. 1–10, 2023.

[9] H. Abumarshoud *et al.*, "LiFi through reconfigurable intelligent surfaces: A new frontier for 6G?" *IEEE Vehicular Technol. Mag.*, vol. 17, no. 1, pp. 37–46, 2022.

[10] C. Chen *et al.*, "Frequency-domain channel characteristics of intelligent reflecting surface assisted visible light communication," *J. Lightw. Technol.*, vol. 41, no. 24, pp. 7355–7369, 2023.

[11] J. Li *et al.*, "Integrated communication and positioning for IRS-assisted LiFi networks," in *2024 IEEE Wireless Commun. & Netw. Conf. (WCNC)*, 2024, pp. 01–06.

[12] B. Clare and D. Kepert, "The closest packing of equal circles on a sphere," *Proc. Roy. Soc. London. A. Math. & Physical Sci.*, vol. 405, no. 1829, pp. 329–344, 1986.